Scientific Research Publishing

Advances in Pure Mathematics, 2024, 14, 118-138
https://www.scirp.org/journal/apm
ISSN Online: 2160-0384
ISSN Print: 2160-0368

Existence of a Hölder Continuous Extension on Embedded Balls of the 3-Torus for the Periodic Navier Stokes Equations

Terry E. Moschandreou

Intermediate Science and Mathematics, TVDSB London Ontario, Canada
Email: tmoschandreou@gmail.com

How to cite this paper: Moschandreou, T.E. (2024) Existence of a Hölder Continuous Extension on Embedded Balls of the 3-Torus for the Periodic Navier Stokes Equations. *Advances in Pure Mathematics*, **14**, 118-138.
https://doi.org/10.4236/apm.2024.142006

Received: January 3, 2024
Accepted: February 26, 2024
Published: February 29, 2024

Copyright © 2024 by author(s) and Scientific Research Publishing Inc.
This work is licensed under the Creative Commons Attribution International License (CC BY 4.0).
http://creativecommons.org/licenses/by/4.0/

Open Access

Abstract

This article gives a general model using specific periodic special functions, which is degenerate elliptic Weierstrass P functions whose presence in the governing equations through the forcing terms simplify the periodic Navier Stokes equations (PNS) at the centers of cells of the 3-Torus. Satisfying a divergence-free vector field and periodic boundary conditions respectively with a general spatio-temporal forcing term which is smooth and spatially periodic, the existence of solutions which have finite time singularities can occur starting with the first derivative and higher with respect to time. The existence of a subspace of the solution space where v_3 is continuous and $\{C, y_1, y_1^2\}$, is linearly independent in the additive argument of the solution in terms of the Lambert W function, ($y_1^2 = y_2$, $C \in \mathbb{R}$) together with the condition $v_2 = -2y_1 v_1$. On this subspace, the Biot Savart Law holds exactly [see Section 2 (Equation (13))]. Also on this subspace, an expression X (part of PNS equations) vanishes which contains all the expressions in derivatives of v_1 and v_2 and the forcing terms in the plane which are related as $F_{T_2} = -2y_1 F_{T_1}$ with the cancellation of all such terms in governing PDE. The y_3 component forcing term is arbitrarily small in ε ball where Weierstrass P functions touch the center of the ball both for inviscid and viscous cases. As a result, a significant simplification occurs with a v_3 only governing PDE resulting. With viscosity present as ν changes from zero to the fully viscous case at $\nu = 1$ the solution for v_3 reaches a peak in the third component y_3. Consequently, there exists a dipole which is not centered at the center of the cell of the Lattice. Hence since the dipole by definition has an equal in magnitude positive and negative peak in y_3, then the dipole Riemann cut-off surface is covered by a closed surface which is the sphere $\|\boldsymbol{r}\| = 1$ and where a

given cell of dimensions $[-1,1]^3$ is circumscribed on a sphere of radius 1. For such a closed surface containing a dipole it necessarily follows that the flux at the surface of the sphere of v_3 wrt to surface normal $\boldsymbol{n}$ is zero including at the points where the surface of sphere touches the cube walls. At the finite time singularity on the sphere a rotation boundary condition is deduced. It is shown that v_3 is spatially finite on the Riemann Sphere and the forcing is oscillatory in y_3 component if the velocity v_3 is. It is true that $\frac{\partial v_3}{\partial \boldsymbol{n}} = \boldsymbol{n} \cdot \nabla v_3$. A boundary condition on the sphere shows the rotation of a sphere of viscous fluid. Finally on the sphere a solution for v_3 is obtained which is proven to be Hölder continuous and it is shown that it is possible to extend Hölder continuity on the sphere uniquely to all of the interior of the ball.

Keywords

Navier-Stokes, PNS, 3-Torus, Periodic, Ball, Sphere, Hölder, Continuous, Riemann-Surface, Uniqueness

1. Introduction

Turbulent flows are characterized by the non-linear cascades of energy and other inviscid invariants across a huge range of scales, from where they are injected to where they are dissipated. In the 3D viscous incompressible flow, the kinetic energy is transferred from large scale eddies to small scale eddies, in particular, if you inject energy at a wavenumber k_F kinetic energy will be transferred to the wavenumbers k s.t. $k > k_F$. In 2D viscous incompressible flow the kinetic energy is transferred from small to large eddies, in particular if you inject energy at wavenumber k_F, then your energy will be transferred both to the larger and smaller wavenumbers, this fact can be flagged as an inverse cascade. This double cascade is due to the presence of two inviscid quadratic invariants: energy and enstrophy. Experimental, numerical and theoretical works have shown that many turbulent configurations deviate from the ideal three and two dimensional homogeneous and isotropic cases characterized by the presence of a strictly direct and inverse energy cascade [1]. It can be assumed that the flow is confined in a periodic box of size L and that the external forcing is acting on a band limited range of scales centered around ℓ_{in}. It is important to discuss the case when the horizontal size, L of the domain is finite and no drag force is present so that a condensate forms in a split cascade regime. With layers of fluid of finite height, there is a path to saturate the inverse cascade. In square boxes the condensate takes the form of a vortex dipole. As the condensate increases in amplitude and is constrained not to exceed the size of the box, its eddy-turn-over-time also increases. Thus, at sufficiently large amplitudes, the rotation rate of the counter-rotating vortex will locally cancel the effects of Ω in the rotating Navier Stokes equations, and the flow will no longer be restricted to 2D dynamics and it

will be able to develop a forward energy cascade. This occurs when the amplitude of the condensate velocity U is such that $U = \Omega L$. The system thus reaches a zero flux state that has a finite inverse flux in the slow manifold dynamics and a forward flux in the 3D fast manifold dynamics [1]. Experimental techniques in interface dynamics of two turbulent fluids are carried out in [2]. Cutting-edge analytical and numerical approaches to the Gilson-Pickering (GP) problem have been carried out in order to get precise solutions. The model explains wave propagation in plasma physics and crystal lattice theory [3]. In physics the dimensions of a massive object can be ignored and can be treated as a pointlike object, *i.e.* a point particle. In electrostatic theory, point particles with electric charge are referred to as point charges. Two point charges, one with charge $+q$ and the other one with charge $-q$ separated by a distance d, constitute an electric dipole. An object with an electric dipole moment p is subject to a torque τ when placed in an external electric field E. In the context of viscous fluid dynamics and at the very heart of turbulent fluid flows are many interacting vortices that produce a chaotic and seemingly unpredictable velocity field. Gaining new insight into the complex motion of vortices and how they can lead to topological changes in flows is of fundamental importance in our strive to understand turbulence. One aim is to form an understanding of vortex interactions by investigating the dynamics of point vortex dipoles [4]. The existence of dipoles describes vortex motion and can possibly lead to a better understanding of the turbulence problem. Dipolar vortices are also self-propagating, which implies some consequences on the transport of mass and heat. For instance, a dipole can trap passive scalars such as phytoplankton [5] within its core, and thereafter transport it. Contrary to the single monopole which is known mathematically to converge towards a Lamb-Oseen vortex by viscous diffusion, this problem seems not to be settled in the case of the dipole. Now on the topic of the well-posedness of solutions to Navier Stokes equations, Wang *et al.* [6] have examined globally dynamical stabilizing effects of the geometry of the domain at which the flow locates and of the geometry structure of the solutions with the finite energy to the three-dimensional 3D incompressible Navier Stokes and Euler systems. The global well-posedness for large amplitude smooth solutions to the Cauchy problem for 3D incompressible NS and Euler equations based on a class of variant spherical coordinates has been obtained, where smooth initial data is not axi-symmetric with respect to any coordinate axis in Cartesian coordinate system. In their work [6] they have considered such variant spherical coordinates with Dirichlet type boundary conditions and have proven the existence, uniqueness and exponential decay rate in time of the global strong solution to the initial boundary value problem for 3D incompressible NS equations for a class of the smooth large initial data. In the present work, it has been determined that as the kinematic viscosity changes from the corresponding value at $\nu = 0$ to the fully viscous case for the Periodic Navier Stokes equations (PNS) at the value $\nu = 1$ the solution reaches a peak ($\frac{\partial v_3}{\partial y_3} = 0$) in y_3 (the third component of

$\boldsymbol{r} = (y_1, y_2, y_3)$ in Cartesian co-ordinates). Here in the viscous case there exists a dipole which is not centered at the center of the cell of the Lattice. This implies that since the dipole by definition has an equal in magnitude positive and negative peak in the third component of velocity, then the dipole Riemann cut-off surface is covered by a closed surface which is the sphere $\|\boldsymbol{r}\| = 1$ and where a given cell of dimensions $[-1,1]^3$ is circumscribed on a sphere of radius 1. For such a closed surface containing a dipole it necessarily follows that the flux at the surface of the sphere of v_3 wrt to surface normal $\boldsymbol{n}$ is zero. In terms of mathematical analysis of the NS equations in a thin spherical shell, the convergence of the longitudinal velocity averaged in the radial direction across the shell to the strong solution to the two-dimensional NS equations on a sphere as the thickness of the shell converges to zero has been rigorously proved in [7]. However a Dirichlet type impenetrability condition is used there with all three components of velocity (no gradients at the wall). In the present work a Neumann impenetrability condition is used with the gradient of the third component of velocity. Here at the six points where the sphere touches the cube walls, it has been determined that the velocities satisfy PNS and the function v_3 is Hölder continuous there. By using the spherical coordinate system in terms of Cartesian co-ordinates and using the chain rule the solution can be extended to all of the sphere. This is the first extension. In terms of pure rotation $(1,1)\cdot\left(\frac{\partial v_1}{\partial y_1}, \frac{\partial v_2}{\partial y_2}\right) = 0$ which signifies rotation of the spheres. Finally as a result of the present work, on the sphere with a Neumann boundary condition, (Here $\frac{\partial v_3}{\partial \boldsymbol{n}} = \boldsymbol{n}\cdot\nabla v_3$) a non smooth solution [8] for v_3 exists which is Hölder continuous and it is proven that it is possible to extend Hölder continuity on the sphere uniquely to all of the interior of the Ball of radius one. Although non-uniqueness is proposed to occur for solutions in the interior of the ball for PNS equations there exists at least one solution there that is Hölder continuous.

2. Materials and Methods

Consider the incompressible 3D Navier-Stokes equations defined on the 3-Torus $\mathbb{T}^3 = \mathbb{R}^3/\mathbb{Z}^3$. The PNS system is,

$$\begin{aligned} &\frac{\partial u}{\partial t} - \Delta u + u\cdot\nabla u = -\nabla p + f \\ &\operatorname{div} u = 0 \\ &u_{t=0} = u_0 \end{aligned} \tag{1}$$

where $u = u(x,y,z,t)$ is velocity, $p = p(x,y,z,t)$ is pressure and $f = f(x,y,z,t)$ is the forcing function. Here $u = (u_x, u_y, u_z)$, where u_x, u_y, and u_z denote respectively the *x*, *y* and *z* components of velocity. Introducing Poisson's equation (see [9] [10] [11]), the second derivative P_{zz} is set equal to the second derivative obtained in the $\mathcal{G}_{\delta_1}$ expression further below, as part of $\mathcal{G}$, and

$$P_{zz} = -2u_z\nabla^2 u_z - \left(\frac{\partial u_z}{\partial z}\right)^2 + \frac{1}{\eta}\frac{\partial}{\partial z}\left(\frac{\partial u_z}{\partial x} + \frac{\partial u_z}{\partial y}\right) - \delta u_x \frac{\partial^2 u_z}{\partial z}\partial x$$
$$- \delta u_y \frac{\partial^2 u_z}{\partial z \partial y} + \left(\frac{\partial u_x}{\partial x}\right)^2 + 2\frac{\partial u_x}{\partial y}\frac{\partial u_y}{\partial x} + \left(\frac{\partial u_y}{\partial y}\right)^2 \tag{2}$$

where the last three terms on rhs of Equation (2) can be shown to be equal to $-\left(P_{xx} + P_{yy}\right)$. Along with equations below, the continuity equation in Cartesian co-ordinates is $\nabla^i u_i = 0$. The one parameter group of transformations on a critical space of PNS is,

$$u_x = \frac{u_x^*}{\delta}; u_y = \frac{u_y^*}{\delta}; u_z = \frac{u_z^*}{\delta}; P = \frac{P^*}{\delta^2}$$
$$x = x^*\delta; y = y^*\delta; z = z^*\delta; t = t^*\delta^2, \tag{3}$$
$$\frac{\partial}{\partial x} = \delta^{-1}\frac{\partial}{\partial x^*}; \frac{\partial}{\partial y} = \delta^{-1}\frac{\partial}{\partial y^*}; \frac{\partial}{\partial z} = \delta^{-1}\frac{\partial}{\partial z^*}; \frac{\partial}{\partial t} = \delta^{-2}\frac{\partial}{\partial t^*}$$

Next the right hand side of the group of transformations Equation (3) is mapped to η variable terms. Here η and δ are in the interval $\delta, \eta \in [1, \infty)$,

$$u_i^* = \frac{1}{\eta}v_i; P^* = \frac{1}{\eta^2}Q; x_i^* = \eta y_i; t^* = \eta^2 s, \ i = 1,2,3. \tag{4}$$

The double transformation here is used for notational clarity. Note that the original Navier-Stokes equations are preserved and rearranged in the following form,

$$\mathcal{G}(\eta) = \mathcal{G}(\eta)_{\delta_1} + \mathcal{G}(\eta)_{\delta_2} + \mathcal{G}(\eta)_{\delta_3} + \mathcal{G}(\eta)_{\delta_4} = 0 \tag{5}$$

where $\mathcal{G}(\eta)_{\delta_i}, i = 1,2,3,4$ are given in [12] and [13] and it has been shown there that this decomposition is valid and that on a volume of an arbitrarily small sphere embedded in each cell of the lattice centered at the central point of each cell of the 3-torus, $\mathcal{G}(\eta)_{\delta_3}$ is negligible for the case of no viscosity (Euler equation) and for viscosity $\nu = 1$ the existence of a dipole occurs with the centre of the dipole occurring shifted away from the centre of the given cell. From this equation we can solve for $\frac{\partial Q}{\partial y_3}$ algebraically and differentiating wrt to y_3 and using Poisson's equation by setting the representation of each of the two partial derivatives wrt to y_3 equal to each other we can obtain,

$$L = 0 \tag{6}$$
$$L = L_1 + L_2 + L_3 \tag{7}$$

where each $L_i, i = 1,2,3$ is given as,

$$L_1 = \left(\frac{\partial v_3}{\partial s}\right)^2 \mu(\delta - 1)\frac{\partial^3 v_3}{\partial y_3 \partial y_1^2} + \left(\frac{\partial v_3}{\partial s}\right)^2 \mu(\delta - 1)\frac{\partial^3 v_3}{\partial y_3 \partial y_2^2}$$
$$+ \left(\frac{\partial v_3}{\partial s}\right)^2 \mu(\delta - 1)\frac{\partial^3 v_3}{\partial y_3^3} + \left(\frac{\partial v_3}{\partial s}\right)(v_3)^2\left(\frac{\partial^3 v_3}{\partial y_3^2 \partial s}\right)\delta\rho$$
$$-(v_3)^2\left(\frac{\partial^2 v_3}{\partial y_3 \partial s}\right)^2 \delta\rho - 2\rho\left(\left(\frac{\delta}{2} - \frac{1}{2}\right)\left(\frac{\partial v_3}{\partial s}\right)^2 - v_3\left(\frac{\partial v_3}{\partial s}\right)\left(\frac{\partial v_3}{\partial y_3}\right)\delta\right.$$

$$+\left(v_3\left(F_{T_1}\left(y_1,y_2,y_3,s\right)+\frac{\partial v_1}{\partial s}\right)\frac{\partial v_3}{\partial y_1}+v_3\left(F_{T_2}\left(y_1,y_2,y_3,s\right)+\frac{\partial v_2}{\partial s}\right)\frac{\partial v_3}{\partial y_2}\right.$$
$$\left.+\frac{1}{2}\Lambda\left(y_1,y_2,y_3,s\right)+\frac{1}{2}\Phi\left(s\right)\right)\delta\Bigg)\frac{\partial^2 v_3}{\partial y_3\partial s}$$

$$L_2=\Bigg(\left(\delta-1\right)\left(\delta v_1\left(y_1,y_2,y_3,s\right)-1\right)\frac{\partial v_3}{\partial s}$$
$$+2v_3\rho\delta\left(F_{T_1}\left(y_1,y_2,y_3,s\right)+\frac{\partial v_1}{\partial s}\right)\Bigg)\times\frac{\partial^2 v_3}{\partial y_3\partial y_1}$$
$$+\Bigg(\left(\delta-1\right)\left(v_2\left(y_1,y_2,y_3,s\right)\delta-1\right)\frac{\partial v_3}{\partial s}$$
$$+2v_3\rho\delta\left(F_{T_2}\left(y_1,y_2,y_3,s\right)+\frac{\partial v_2}{\partial s}\right)\Bigg)\times\frac{\partial^2 v_3}{\partial y_3\partial y_2}$$
$$+3v_3\left(-\frac{2}{3}+\left(\rho+\frac{2}{3}\right)\delta\right)\left(\frac{\partial v_3}{\partial s}\right)\frac{\partial^2 v_3}{\partial {y_3}^2}+\cdots$$

$$L_3=2v_3\left(\frac{\partial v_3}{\partial s}\right)\left(\delta-1\right)\frac{\partial^2 v_3}{\partial {y_1}^2}+2v_3\left(\frac{\partial v_3}{\partial s}\right)\left(\delta-1\right)\frac{\partial^2 v_3}{\partial {y_2}^2}+2\left(\frac{\partial^2 v_1}{\partial y_3\partial s}\right)v_3\left(\frac{\partial v_3}{\partial y_1}\right)\rho\delta$$
$$+2\left(\frac{\partial^2 v_2}{\partial y_3\partial s}\right)v_3\left(\frac{\partial v_3}{\partial y_2}\right)\rho\delta+\Bigg(\left(-1+\left(3\rho+1\right)\delta\right)\left(\frac{\partial v_3}{\partial y_3}\right)^2+\left(\delta-1\right)$$
$$\times\left(\left(\frac{\partial v_1}{\partial y_1}\right)^2+2\left(\frac{\partial v_1}{\partial y_2}\right)\frac{\partial v_2}{\partial y_1}+\left(\frac{\partial v_2}{\partial y_2}\right)^2\right)\Bigg)\frac{\partial v_3}{\partial s}$$
$$+2\rho\Bigg(\Bigg(\left(F_{T_1}\left(y_1,y_2,y_3,s\right)+\frac{\partial v_1}{\partial s}\right)\frac{\partial v_3}{\partial y_1}+\left(\frac{\partial v_3}{\partial y_2}\right)\left(F_{T_2}\left(y_1,y_2,y_3,s\right)+\frac{\partial v_2}{\partial s}\right)\Bigg)\frac{\partial v_3}{\partial y_3}$$
$$+v_3\left(\frac{\partial v_3}{\partial y_1}\right)\frac{\partial F_{T_1}}{\partial y_3}+v_3\left(\frac{\partial v_3}{\partial y_2}\right)\frac{\partial F_{T_2}}{\partial y_3}+\frac{1}{2}\frac{\partial\Lambda\left(y_1,y_2,y_3,s\right)}{\partial y_3}\Bigg)\delta\Bigg]\frac{\partial v_3}{\partial s}$$

$$\Lambda\left(y_1,y_2,y_3,s\right)=2\frac{f_0\left(s\right)F\left(y_1,y_2,y_3\right)v_3\left(y_1,y_2,y_3,s\right)\dfrac{\partial v_3}{\partial y_1}}{\delta}$$
$$+2\frac{f_0\left(s\right)G\left(y_1,y_2,y_3\right)v_3\left(y_1,y_2,y_3,s\right)\dfrac{\partial v_3}{\partial y_2}}{\delta}$$
$$-\delta^3 v_3\left(\frac{\partial v_3}{\partial y_3}\right)F_{sz}\left(y_1,y_2,y_3,s\right)$$
$$+\delta^2\left(\left(\frac{\partial v_3}{\partial y_3}\right)F_{sz}\left(y_1,y_2,y_3,s\right)+v_3\frac{\partial F_{sz}}{\partial y_3}\right) \tag{8}$$

where $\boldsymbol{f}=\left(F_{T_1},F_{T_2},F_{sz}\right)$ is the external forcing vector and $\boldsymbol{v}=\left(v_1,v_2,v_3\right)$ is the velocity in each cell of the 3-Torus.

For the three forcing terms, set them equal to products of reciprocals of degenerate Weierstrass P functions shifted in spatial co-ordinates from the center

$(a_i, b_i, c_i), i = 1, \cdots, N$.

The (a_i, b_i, c_i) is the center of each cell of the lattice in $\mathbb{T}^3$. Upon substituting the Weierstrass P functions and their reciprocals into Equations (6) and (7) together with the forcing terms given by Λ (in Equation (8)), it has been determined that in the equation terms in it are multiplied by reciprocal P functions that touch the centers of the cells of the lattice thus simplifying Equations (6) and (7). The initial condition in v_3 at $s = 0$ is instead of a product of reciprocal degenerate P function for forcing, is a sum of these functions. The parameter m in the P function if chosen to be small gives a ball,

$$B_r = \left\{ y \in \mathbb{R}^3 : \left\| y \right\|_2 = \left(\left\| y_1 \right\|^2 + \left\| y_2 \right\|^2 + \left\| y_3 \right\|^2 \right)^{\frac{1}{2}} \le r \right\} \tag{9}$$

In the case when fluid region Ω has a connected boundary and certain smoothness conditions are fulfilled, Leray proved the solvability of the Navier Stokes equations in his famous paper [14]. The same result holds when the flux Fl_i of the velocity vector (all 3 components of velocity) across each connected component Γ_i of the boundary vanishes. This condition means that the flow region contains neither sources nor sinks.

Now continuing the analysis, the function Φ associated with $\mathcal{G}(\eta)_{\delta_3}$ in [12] and [13] can be calculated as follows,

$$\begin{aligned} \Phi = & \frac{2}{3}\left(F_4(t)\right)^2 C_a(t)\,\text{EllipticE}\left(\text{JacobiSN}\left(1+C, i\right), i\right) R \\ & + \frac{2}{3} R F_4(t) C_a(t)\left(-F_4(t)\,\text{EllipticE}\left(\text{JacobiSN}\left(-1+C, i\right), i\right) + 6C - 2F_4(t)\right) \end{aligned} \tag{10}$$

where $C_a(t)$ are pressure gradient derivative terms wrt to x, y and z as functions of t.

Solutions of Equations (6) and (7) exist in the form $v_3 = F_4(t) F_5(\boldsymbol{x})$ where the function Φ can be explicitly written as

$$\Phi = -\frac{F_4(t)\left(F_4(t)\left(\frac{\mathrm{d}}{\mathrm{d}t} F_4(t) \right)^2 - \left(\frac{\mathrm{d}}{\mathrm{d}t} F_4(t) \right)^2 \mu \right)}{\left(\frac{\mathrm{d}}{\mathrm{d}t} F_4(t) \right) \lambda^2 \rho} \tag{11}$$

where λ is the corresponding eigenvalue associated with the solution of Equations (6) and (7). Setting the two functional forms for Φ equal to each other and solving the ordinary differential equation for $F_4(t)$ (see [12] and [13]), a LambertW function solution exists for $F_4(t)$ and the form of solution is a W function multiplied by a JacobiSN complex valued function in $\boldsymbol{x}$ (see [13]-chapter 8).

It has recently been shown in [12] that the following PDE results on a suitable subspace of the solution space for v_3 which holds on an epsilon ball about the center of each cell of the lattice and existing (to be shown) dipole center of a given cell of $\mathbb{T}^3$,

$$\left(\frac{\partial v_3}{\partial s}\right)^2\left(\frac{\partial^3 v_3}{\partial y_3^3}+\frac{\partial^3 v_3}{\partial y_3\partial y_2^2}+\frac{\partial^3 v_3}{\partial y_3\partial y_1^2}\right)\mu(\delta-1)$$
$$+\frac{1}{3}\left(\frac{\partial v_3}{\partial s}\right)^2(2\delta-2)v_3\left(\frac{\partial^2 v_3}{\partial y_3^2}+\frac{\partial^2 v_3}{\partial y_2^2}+\frac{\partial^2 v_3}{\partial y_1^2}\right) \tag{12}$$
$$+\frac{1}{6}\left(3\rho v_3\frac{\partial^2 v_3}{\partial y_3^2}+3\left(\frac{\partial v_3}{\partial y_3}\right)^2\rho-\left(\frac{\partial v_3}{\partial y_3}\right)^2+\frac{\partial^2 v_3}{\partial y_3\partial y_1}+\frac{\partial^2 v_3}{\partial y_3\partial y_2}\right)\frac{\partial v_3}{\partial s}=0$$

Using the definition of vorticity in the y_3 direction it follows that in the subspace where $X=0$ in [12] that the following PDE occurs,

$$-2\left(v_1(y_1,y_2,y_3,s)-1\right)-2\frac{\partial v_1}{\partial y_1}-\frac{\partial v_1}{\partial y_2}=-\ln\left(F\left(-y_1+y_2,y_3,s\right)\right)=\omega_3 \tag{13}$$

with solution

$$v_1=\frac{1}{2}\left[\int^{y_1}\left[-1+\ln\left(F\left(-a/2-y_1/2+y_2,y_3,s\right)\right)\right]\mathrm{e}^a\mathrm{d}a\right.$$
$$\left.+2F_1\left(-y_1/2+y_2,y_3,s\right)\right]\mathrm{e}^{-y_1} \tag{14}$$

It is evident that at $y_1=a$, and $F_1=-\int^{y_1}\frac{1}{2}\ln\left(\frac{\left|-y_1/2+y_2\right|^3}{-y_1/2+y_2}\right)\mathrm{d}a$ and using division property of logarithm function and the fact that locally near 1, $\ln(Z)=Z-1$ that,

$$v_1=\int^{y_1}\left(\frac{\left(-1+\ln\left[F\left(y_2-y_1\right)\right]+\ln(e)\right)\left(-a/2+y_2\right)}{\left|a/2-y_2\right|^3\mathrm{e}^{-2a}}-1\right)\mathrm{d}a$$

and

$$v_1=\int^{y_1}\left(\frac{\left(\ln\left[F\left(y_2-y_1\right)\right]\right)\left(-a/2+y_2\right)}{\left|a/2-y_2\right|^3\mathrm{e}^{-2a}}-1\right)\mathrm{d}a$$

Here it is seen that the Biot-Savart Law is established on $\mathcal{J}_{y_3,s}$ space in [12]. It is assumed that the velocity v_1 is shifted by negative 1. Transforming back to $*$ variables the e^{-2a} term will be equal to one when δ is large. Also it has been computed that the cross-product,

$$\left(y_1-a/2,y_2-a/2,y_3-a/2\right)\times\left(\omega_1,\omega_2,\omega_3\right)$$
$$=\begin{bmatrix}\left(y_2-a/2\right)F\left(-y_1+y_2,y_3,s\right)-\left(y_3-a/2\right)\omega_2\\-\left(y_1-a/2\right)F\left(-y_1+y_2,y_3,s\right)+\left(y_3-a/2\right)\omega_1\\\left(y_1-a/2\right)\omega_2-\left(y_2-a/2\right)\omega_1\end{bmatrix}$$

Considering the first row of this matrix establishes the result given by v_1 formula. Note that the integral of 1 is *a* which approaches zero in $*$ variables since a division by δ results and for large δ.

3. Results

The solution in [12] occurs for large ζ and time *t*. The solution was rescaled

in ζ. (In the form $\zeta = -\zeta + \alpha$, where α is a large complex valued shift.) In [12] this was valid for $\nu = 0$ that is the Euler equations. In this paper the same shift occurs but as ν approaches unity and given the reduced PNS equations the relationship in terms of the definition of the LambertW function as shown in Equation (16) exists. The variable ζ is complexified. As a result the first derivative wrt to z^* can be written using the chain rule as,

$$\frac{\partial v_3}{\partial z^*} = \frac{\partial v_3}{\partial \zeta}\frac{\partial \zeta\left(z^*\right)}{\partial z^*} \tag{15}$$

Here it is assumed that $\zeta = \zeta\left(z^*\right)$, where ζ is arbitrary large complex valued data in the complex norm in the complex space $\mathbb{C}$. (The test value of the form of this function turns out to be $\zeta = \zeta\left(z^*\right) = \frac{B}{z^* - c_i}$, where B is precisely determined to produce the Riemann surface further obtained and c_i, $i = 1,2$ where central point occurs for $c_1 = 0$ and c_2 is the dipole off center point for high viscosity. There are two ε balls, one about the origin with associated low viscosity and one about the shifted away from origin dipole center associated with high viscosity). Also the variable z^* is the complexification of the z^* -component of velocity given by PNS equations on $\mathbb{T}^3$. (recall one can use either z^* or y_3 or u_z^* or v_3 with a factor of δ introduced. It can be shown that as ζ gets large $\frac{\partial v_3}{\partial \zeta} \to 0$. Also note $\delta \neq 1$ for the viscous case).

The argument of the shifted Riemann surface obtained is derived from the definition of the LambertW function. The argument of the W function which is a function of ζ, say $Q(\zeta)$ is set equal to we^w. It is precisely as follows,

$$\begin{aligned} &1.0\ln\left(0.000843648\zeta - 8.280128000\right) + 9.292505600 \\ &- 0.0008436480000\zeta = \ln\left(we^w\right) + 1 \end{aligned} \tag{16}$$

When the logarithm terms are subtracted the other terms are put to the right hand side of the equation. Taking the exponential of both sides cancels the logarithm and leaves us with an exponential of a binomial in $\zeta = \zeta\left(z^*\right)$. Linearizing the exponential gives the dipoles in **Figure 1** and **Figure 2**. The "plot3d" command is used where four functions are plotted together, that is, $x = \mathrm{Re}(\zeta)$, $y = \mathrm{Im}(\zeta)$, u and v, where $w = u + iv$. Here w is the complex LambertW function associated with the viscous solution. One solves for ζ in terms of u, v.

The command lines in Maple are:

$$1.000000000 * \ln(0.843648e-3 * \zeta - 8.280128000) + 9.292505600 - 0.8436480000e-3 * \zeta = \ln(w * \exp(w)) + 1;$$

$$\zeta := (0.1517220452e-1 * (647852. * w * \exp(w) - 646885.)) / (w * \exp(w) - 1.);$$

$$w := u + I * v;$$

$$x := evalc(Re(\zeta));$$

$$y := evalc(Im(\zeta));$$

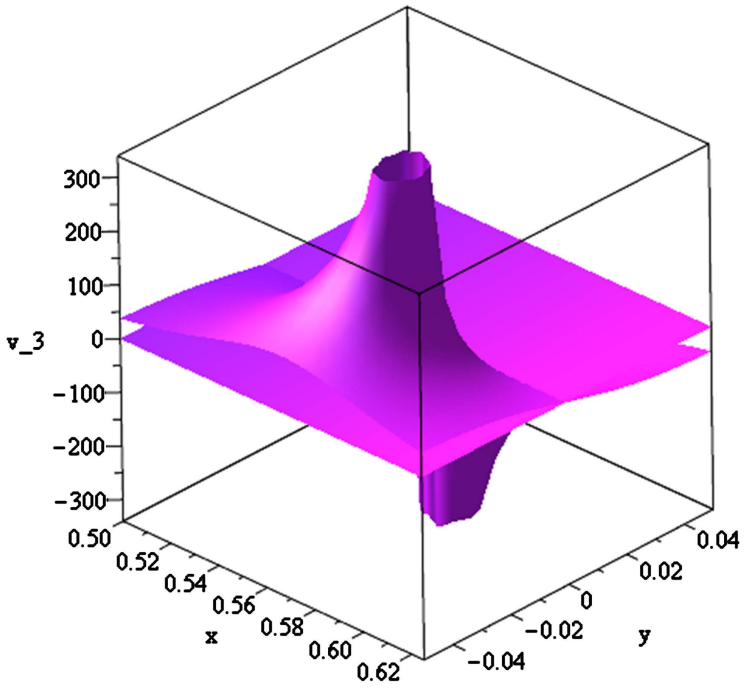

Figure 1. Positive peak in the dipole for Maple plot of Riemann surface of velocity v_3.

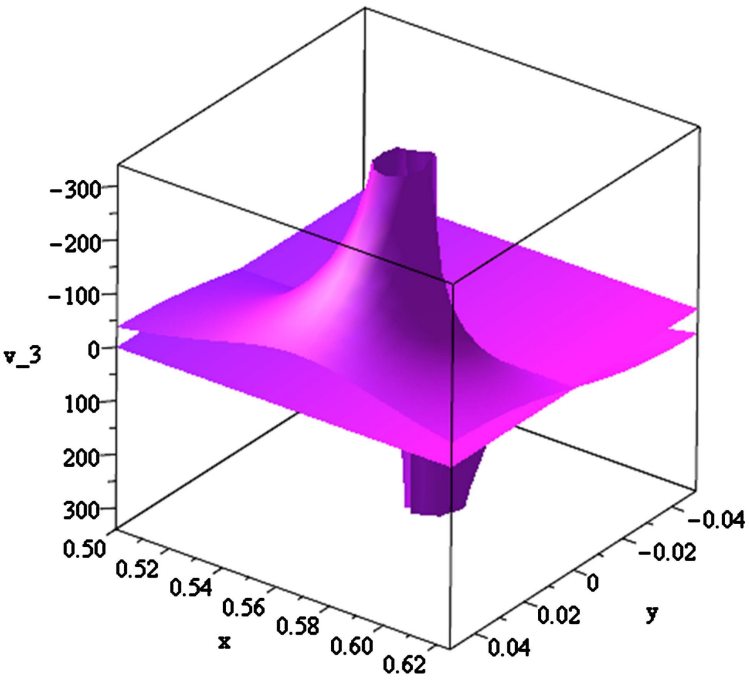

Figure 2. Negative peak in the dipole for Maple plot of Riemann surface of velocity v_3.

$$plot3d([x,y,u,v],u=-1.21..1.21,v=-1.21..1.21,axes=BOX,$$
$$orientation=[-110,73],$$
$$labels=["x","y","v"],style=PATCHNOGRID,colour=u,$$
$$view=[-1..1,-1..1,-25..25],grid=[60,60].);$$

Note that we use the following: Given a constant c we can solve $cwe^{w} = X$ simply by solving $we^{w} = X/c$ which says $w = W(X/c)$, W is the LambertW function. The values are large in v_3 for viscous flows but become physical when we divide by $\delta \gg 1$. In **Figure 3** the quantity is scaled down by dividing by an appropriate large δ. Here the Riemann surface is centralized for small time s and very small viscosity in comparison to the viscosity shown in **Figure 1** and **Figure 2** where an offset center exists of a dipole. For the (arbitrary) small viscosity this occurs near the center of the sphere. For low viscosity compared to the higher viscosity case, a finite time singularity occurs well before the higher viscous case. In the first command line of the previous program, taking the negative of both sides and then operating by the exponential function gives on the left side the argument of the LambertW function solution to the viscous problem.

The vanishing of the derivative of v_3 wrt to y_3 is connected to Rummer and Fet's theory [15] of expressing the volume integral of the Laplacian on an epsilon ball, where in Equation (17) the following reduced PDE occurs when viscosity is included in the PNS equations and thus the reduced form obtained,

$$\begin{aligned} &-\left(\frac{\partial v_3}{\partial s}\right)\left(\frac{1}{2}\rho v_3 \frac{\partial^2 v_3}{\partial y_3{}^2} + \frac{1}{2}\left(\frac{\partial v_3}{\partial y_3}\right)^2 \rho + \frac{1}{6}\frac{\partial^2 v_3}{\partial y_3 \partial y_1} + \frac{1}{6}\frac{\partial^2 v_3}{\partial y_3 \partial y_2}\right) \\ &-(\delta - 1)\left(\frac{\partial v_3}{\partial s}\right)^2 \left(\left(\frac{\partial v_3}{\partial y_1}\right)^2 + \left(\frac{\partial v_3}{\partial y_2}\right)^2 + \left(\frac{\partial v_3}{\partial y_3}\right)^2\right) = 0 \end{aligned} \tag{17}$$

Here the viscosity term is not taken to be zero but the gradient of omitted term in the derivative of v_3 wrt to y_3 vanishes itself. This is due to the chain rule and the large shift in the initial condition in ζ. As a result dividing by viscosity $\mu \neq 0$, the following equation is introduced,

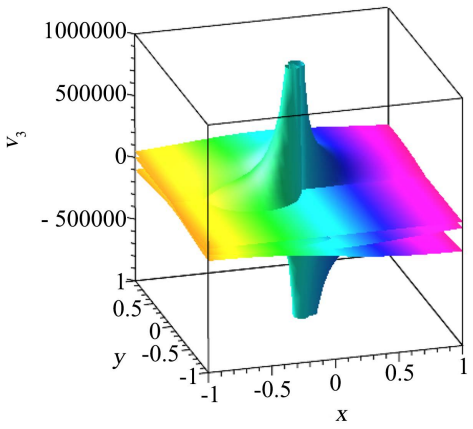

Figure 3. Pair of equal and opposite dipoles at central location for $\mu = 1e-5$ and $\rho = 1000$. Here the Dipole center is near the origin of sphere circumscribed in cube of dimensions $[-1,1]^3$. Shown is the Maple plot of Riemann surface of velocity v_3. Here as shown in [12], the result shows a singularity near the origin for the first derivative in time s. The singularity for small kinematic viscosity occurs at s much sooner than in **Figure 1** and **Figure 2** for the offset high viscosity centre case.

$$\frac{\delta-1}{\mu}\left(\frac{\partial v_3}{\partial s}\right)^2=\kappa \tag{18}$$

$$v_3(y_1,y_2,y_3,s)=-\frac{\sqrt{(\delta-1)\kappa\mu}s}{\delta-1}+F_1(y_1,y_2,y_3) \tag{19}$$

Now it has been pointed out in Chapter 8 of reference [12] and [13] that since δ approaching 1 from the right of 1 provides us with a blowup at minus infinity from the right side of some $t=T^*$ with linear graphs intersecting arbitrarily large v_3 values at $s=0$, that it remains to show that the simplified equation, Equation (17), with κ introduced in place of the derivative term squared has a solution which is Hölder continuous and whose solution has a first derivative blowup from the left at blowup point $t=T^*$. This has already been shown in [12]. Taking $\nu=1$, we have full viscosity in the PNS problem as expected. In [12] the solution was in terms of a LambertW function and for zero viscosity. Here it is seen that as ν goes from 0 to 1 that the the solution v_3 has a derivative in y_3 which approaches zero. In **Figure 1** and **Figure 2** and **Figure 4** the Riemann surfaces are obtained using Maple for the complexification of the solution in terms of the initial condition ζ and large t determined (also see [16] on how to obtain the Maple plots of general Riemann surfaces using the "charisma function" Note that **Figure 4** is a contour plot of the Riemann surface of v_3.).

In the foregoing analyses a matching of two solutions for v_3 and hence $F_4(s)$ has been carried out. One solution is the extended solution in [12] in which a LambertW solution is obtained as a function of a linear combination of spatial and time variables respectively and particularly for the shifted large data ζ problem. The second solution is determined to be as in [13] which is the product of a JacobiSN function and a different form of a time dependent function. This is denoted as $F_4(s)$. Equating the two forms of the $F_4(s)$ functions' LambertW arguments obtained yields,

$$\begin{aligned}
&-2R\rho\lambda^2\left(\text{EllipticE}\left(\text{JacobiSN}(2,i),i\right)-2\right)^2\int_0^t C_a(s)s\text{d}s\\
&+\left(2\int_0^t C_a(s)\text{d}sR\lambda^2\rho t+3C_1t-3C_2\right)\left(\text{EllipticE}\left(\text{JacobiSN}(2,i),i\right)\right)^2\\
&+\left(-8\int_0^t C_a(s)\text{d}sR\lambda^2\rho t-12C_1t+12C_2\right)\text{EllipticE}\left(\text{JacobiSN}(2,i),i\right)\\
&+8\int_0^t C_a(s)\text{d}sR\lambda^2\rho t+12C_1t-12C_2-18\\
&=1.0\ln\left(0.000843648t-8.280128000\right)+9.292505600-0.000843648t
\end{aligned} \tag{20}$$

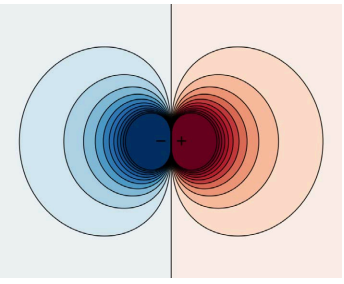

Figure 4. A Dipole pair associated with a contour plot of y_3-component velocity v_3.

The incomplete elliptic integral EllipticE is defined as,

$$\text{EllipticE}(z,k)=\int_0^z \frac{\sqrt{-k^2t^2+1}}{\sqrt{-t^2+1}}\text{d}t \tag{21}$$

Differentiating twice and solving for $C_a(t)$ gives,

$$\begin{aligned} C_a(t) = -21720640.50\Big[& R\rho\lambda^2\Big(\left(-100493511.7-2.812791480\times10^{-23}i\right)t^2 \\ & +\left(1972621614000.0+5.521324887\times10^{-19}i\right)t \\ & +7058091538000000.0-2.709499507\times10^{-15}i \\ & +173765124.0t^2-3410895228000.0t\Big)\Big]^{-1} \end{aligned} \tag{22}$$

Here the constant R and λ^2 is such that,

$$R\lambda^2 \approx 1 \tag{23}$$

In particular R is chosen to be extremely small and λ is very large and as a benchmark test the values considered are,

$$R=1.225\text{e}-37 \tag{24}$$

$$\lambda=0.1\text{e}19 \tag{25}$$

$$C_2=1 \tag{26}$$

$$C_1=0.1\text{e}-1 \tag{27}$$

$$C=1 \tag{28}$$

$$\rho=1 \tag{29}$$

where these values are substituted in the left side of Equation (20). (C = 1 is set in Equation (10) for the function Φ) This temporal solution for the function $F_4(t)$ can be identified as a Hölder continuous function as shown in **Figure 5**.

In the viscous case there exists a dipole which is not centered at the center of the cell of the Lattice. This immediately implies that since the dipole by definition has an equal in magnitude positive and negative peak in the third component of velocity, then the dipole Riemann cut-off surface is covered by a closed surface which is the sphere $\|\boldsymbol{r}\|=1$ and where a given cell of dimensions $[-1,1]^3$ is circumscribed on a sphere of radius 1. See **Figure 6**. For such a closed surface containing a dipole it necessarily follows that the flux at the surface of the sphere of v_3 wrt to $y_i, i=1,2,3$ is zero. Finally as a result on the sphere a solution for v_3 is obtained which is proven to be Hölder continuous and it is proven that it is possible to extend Hölder continuity on the sphere to all of the interior of the sphere.

Recalling the Weierstrass P function (P) based v_1, v_2 and F_{sz} solutions in y_1, y_2 and y_3 co-ordinates.

The governing PDE at the boundary of Ω of the sphere is directly determined from Equations (6) and (7) and the zero flux condition since the ball contains a dipole, where all the derivatives $\frac{\partial v_3}{\partial y_i}, i=1,2,3$ are taken to be zero. The resulting PDE in Cartesian co-ordinates is,

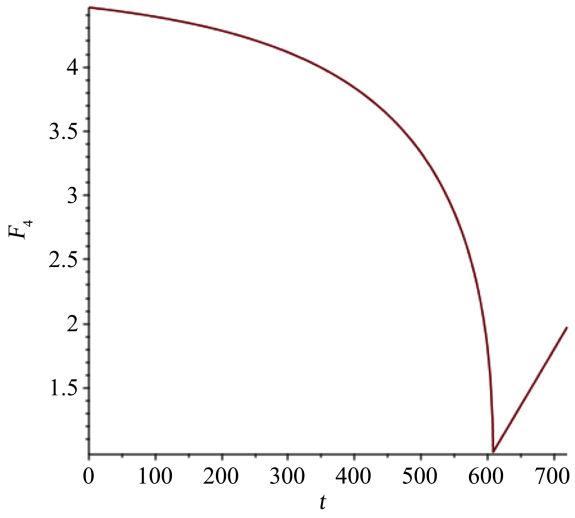

Figure 5. Plot of Hölder continuous function via matching.

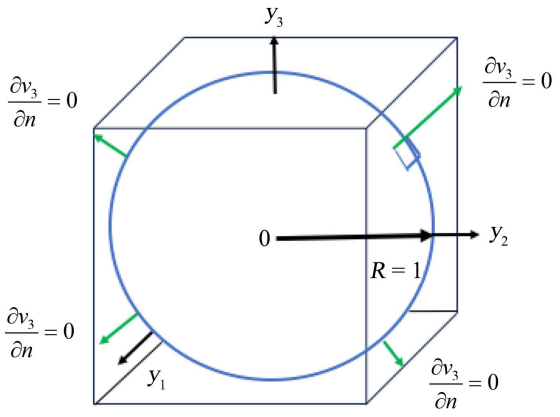

Figure 6. A cube cell $[-1,1]^3$ circumscribed on a sphere of radius 1.

$$\begin{aligned}&(\delta-1)\left[\left(\frac{\partial v_1}{\partial y_1}\right)^2+2\left(\frac{\partial v_1}{\partial y_2}\right)\frac{\partial v_2}{\partial y_1}+\left(\frac{\partial v_2}{\partial y_2}\right)^2\right]\frac{\partial v_3}{\partial s}\\&+\frac{1}{2}\left(\frac{\partial v_3}{\partial s}\right)\left[\delta^2\left(\frac{\partial v_3}{\partial y_3}\right)\frac{\partial F_{sz}}{\partial y_3}+\delta^2 v_3\frac{\partial^2 F_{sz}}{\partial y_3^2}+\delta\rho v_3^2\frac{\partial^3 v_3}{\partial y_2^2\partial s}\right]=0\end{aligned}\tag{30}$$

$$(\delta-1)\left[\left(-\frac{\partial v_3}{\partial y_3}\right)^2\right]\frac{\partial v_3}{\partial s}+\frac{1}{2}\left(\frac{\partial v_3}{\partial s}\right)\left[\delta^2\left(\frac{\partial v_3}{\partial y_3}\right)\frac{\partial F_{sz}}{\partial y_3}+\delta^2 v_3\frac{\partial^2 F_{sz}}{\partial y_3^{\,2}}+\delta\rho v_3^2\frac{\partial^3 v_3}{\partial y_2^2\partial s}\right]=0$$

For Hölder continuous function $F_4(s)$ the corresponding solution is,

$$v_3=F(y_3)F_4(s)\left(A+P\left(y_1,3m^2,m^3\right)^{-1}\right)\times\left(A+P\left(y_2,3m^2,m^3\right)^{-1}\right),\tag{31}$$

and $F_4(s)$ is Hölder.

Here $F_4(s)=(s-s_0)^{\frac{1}{2}}$.

This implies that the forcing F_{sz} is smooth in s and spatial variables since on the Riemann Sphere $x^2=-A$ and $y^2=A$ for A negative. In this case the so-

lution $F_{sz} \in C^{\infty}$ for spatio-temporal variables. Substituting the form of Equation (31) for v_3 into the PDE above gives,

$$F_{sz}(y_1, y_2, y_3, s) = F_1(y_1, y_2, s) \int F(y_3) \mathrm{d}y_3 + F_2(y_1, y_2, s) \tag{32}$$

Let

$$F(y_3) = \alpha \frac{\partial^3}{\partial y_3^3} \log\left(\frac{\partial}{\partial y_3} S_i\left[W\left(-\mathrm{e}^{-(y_3+2)+C} \right) \right] \right) \tag{33}$$

where W is the Lambert W function.

$$S_i(w) = \int \frac{\sin(w)}{w} \mathrm{d}w$$

Plotting the y_3 part produces an oscillatory solution wrt to y_3 provided the constant $C = C_L$ which is indexed by the box size of the cell of Lattice is proportional to the finite number of such cells and is sufficiently large. Also at the poles of the Riemann sphere at $y_3 = 0$ and $y_3 = \infty$ the solution of v_3 in terms of the reciprocal of $F(y_3)$ is finite. The PDE above has as solution a Hölder continuous function in v_3 at six points where the surface of the sphere coincides with the boundary of a given open cube. This must be the solution on the sphere boundary which is therefore Hölder continuous. This follows since we have the following co-ordinate transformations between Cartesian and spherical co-ordinates,(see Figure 7) It is relatively straightforward to show by using the chain rule and the above transformations on the surface of the sphere that the new function v_3 in terms of (r, θ, ϕ, t) is separable on the surface of the sphere and thus is in the same Hölder continuous form as the six points mentioned that are known to be Hölder continuous in s there.

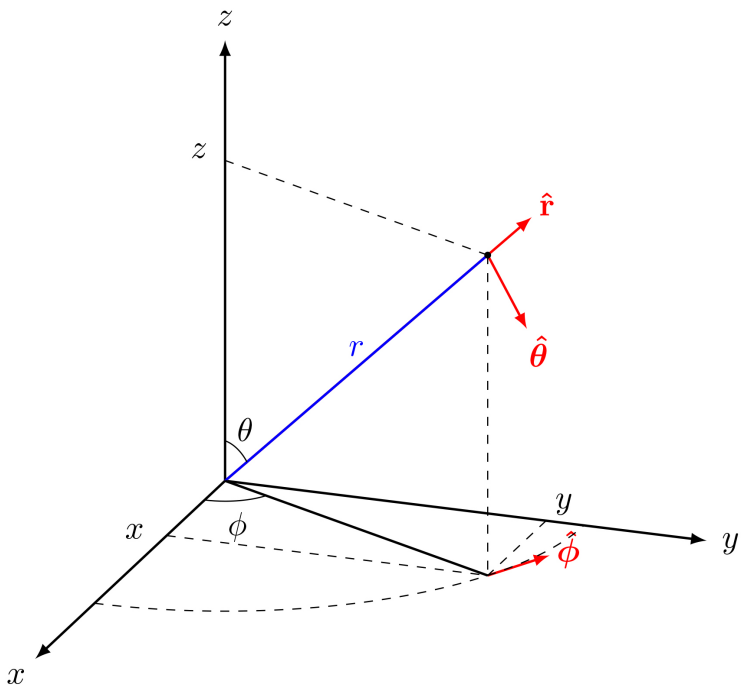

Figure 7. Spherical co-ordinate system associated with transformations to prove that Hölder continuity holds on sphere (TikZ.net [A.Tsagkaropoulos]).

$$\begin{pmatrix} r \\ \theta \\ \phi \end{pmatrix} = \begin{cases} \sqrt{x^2+y^2+z^2} & \\ \begin{cases} \arccos\left(\frac{z}{r}\right) = \arctan\left(\frac{\sqrt{x^2+y^2}}{z}\right) & \text{if } z>0 \\ \pi + \arctan\left(\frac{\sqrt{x^2+y^2}}{z}\right) & \text{if } z<0 \\ \frac{\pi}{2} & \text{if } z=0 \text{ and } xy \neq 0 \\ \text{undefined} & \text{if } x=y=z=0. \end{cases} & \\ \operatorname{sgn}(y)\arccos\left(\frac{x}{\sqrt{x^2+y^2}}\right) = \begin{cases} \arctan\left(\frac{y}{x}\right) & \text{if } x>0 \\ \arctan\left(\frac{y}{x}\right)+\pi & \text{if } x<0 \text{ and } y\geq 0 \\ \arctan\left(\frac{y}{x}\right)-\pi & \text{if } x<0 \text{ and } y<0 \\ \frac{\pi}{2} & \text{if } x=0 \text{ and } y>0 \\ -\frac{\pi}{2} & \text{if } x=0 \text{ and } y<0 \\ \text{undefined} & \text{if } x=y=0. \end{cases} \end{cases}$$

It is relatively straightforward to show by using the chain rule and the above transformations on the surface of the sphere that the new function v_3 in terms of (r,θ,ϕ,t) is separable on the surface of the sphere and thus is in the same Hölder continuous form as the six points mentioned earlier that are known to be Hölder continuous in *s* there.

4. Main Theorem

Finally on the sphere a solution for v_3 is obtained which is proven to be Hölder continuous. It is next proven that it is possible to extend Hölder continuity on the sphere uniquely to all of the interior of the ball.

Theorem 1. Let $\Omega \subseteq \mathbb{R}^n$ be a smooth domain and suppose $f \in C^{\alpha}(\partial\Omega)$, where $\alpha \in (0,1)$. Then there exists a function $\tilde{f} \in C^{\alpha}(\bar{\Omega})$ so that $\tilde{f} \mid \partial\Omega \equiv f$.

Proof of Theorem 1. The following fact is used

$$|x_1 - x_2|^{\alpha} \leq \left(|x_1 - x_3| + |x_2 - x_3|\right)^{\alpha} \leq |x_1 - x_3|^{\alpha} + |x_2 - x_3|^{\alpha}.$$

Let $E \subseteq \mathbb{R}^n$ and let $f : E \to \mathbb{R}$ be such that $|f(x) - f(y)| \leq M|x-y|^{\alpha}$. for all $x, y \in E$. Define:

$$h(x) := \inf\left\{f(y) + M|x-y|^{\alpha} : y \in E\right\},\ x \in \mathbb{R}^n.$$

If $x \in E$, then setting $y = x$ one gets that $h(x) \leq f(x)$. To prove that $h(x)$ is finite for every $x \in \mathbb{R}^n$, we fix $y_0 \in E$. If $y \in E$ then:

$$f(y) - f(y_0) + M|x-y|^{\alpha} \geq -M|y-y_0|^{\alpha} + M|x-y|^{\alpha} \geq -M|x-y_0|,$$

where we have used the fact that if $a \leq 0$ and $b \geq 0$ then $a \leq b$.

And so

$$h(x)=\inf\left\{f(y)+M|x-y|^{\alpha}: y\in E\right\}\geq f(y_0)-M|x-y_0|^{\alpha}>-\infty.$$

Note that if $x\in E$, then we can choose $y_0:=x$ in previous inequality to obtain $h(x)\geq f(x)$. Thus $h(x)\geq f(x)$. Thus h extends f.

Next it is proven that

$$|h(x_1)-h(x_2)|\leq M|x_1-x_2|^{\alpha},$$

for all $x_1,x_2\in\mathbb{R}^n$.

Given $\varepsilon>0$, by the definition of h there exists $y_1\in E$ such that,

$$h(x_1)\geq f(y_1)+M|x_1-y_1|^{\alpha}-\varepsilon.$$

Since $h(x_2)\leq f(y_1)+M|x_2-y_1|^{\alpha}$, we get

$$\begin{aligned}h(x_1)-h(x_2)&\geq M|x_1-y_1|^{\alpha}-M|x_2-y_1|^{\alpha}-\varepsilon\\&\geq -M|x_1-x_2|^{\alpha}-\varepsilon.\end{aligned}$$

Letting $\varepsilon\to 0$ gives

$$h(x_1)-h(x_2)\geq -M|x_1-x_2|^{\alpha}.$$

Finally interchanging the roles of x_1 and x_2 proves that h is Hölder continuous.

□

Finally there is a theorem in ([17] Problem 13 Section 18) that proves the unique determination for the extension of $f:A\to Y$ into the closure of A. The statement of the theorem without proof is given here.

Theorem 2. Let $A\subseteq X$. Let $F:A\to Y$ be continuous. Let Y be a Hausdorff space. Then f can be extended to a continuous function $g:\bar{A}\to Y$ and g is uniquely determined by f.

So there is an extension to the interior of the boundary where the PNS equations hold. So working backwards there exists an extension for the function defined on the interior of the sphere to the closure of the interior of the sphere thereby extending to the ball of radius 1.

5. Discussion

The fundamental idea of the present work is that of how external forces can lead to order in turbulent flow and in particular for the 3D Periodic Navier Stokes equations. The Turbulence problem is an open and important current problem. What is turbulence? Turbulence is disorder and fluctuation. The nonlinear 3D Navier Stokes equations have been addressed in this paper through a sequence of earlier works by the corresponding author of the present paper. When turbulence arises, even if we could see these flows, it is difficult to discern any order in the whirling currents and eddies they contain. Michael Schatz at the Georgia Institute of Technology in Atlanta has recently shown with experiments and simulations that flow patterns with a surprising amount of order can underlie turbu-

lent flow. Prediction of turbulence is very difficult to do, however they showed that there are ordered structures when conducting experiments in the lab [18]. To predict the complex spatio-temporal dynamics of turbulence is a daunting task however some order is possible in the 3-Torus. The existence of a sphere centered at each point of each cell of the lattice $\mathbb{T}^3$ with a Neumann zero flux condition as proven in this paper shows that there is some order in turbulent flow. We know this since for the flux of v_3, 3'rd component of velocity, it is zero and $\frac{\partial v_1}{\partial y_1} = -\frac{\partial v_2}{\partial y_2}$ on the sphere at the singular point in time. Note that on the surface of the sphere, in 2D $(1,1)\cdot\left(\frac{\partial v_1}{\partial y_1}, \frac{\partial v_2}{\partial y_2}\right) = 0$ which signifies rotation of the sphere (Taylor Green Vortex solves this for example) together with the flux of third component of velocity, v_3 at the north and south pole of the sphere. As an analogy, if we consider the dynamics of rotating (about planet's axes) planetary motion and keep in mind that the spherical shapes of the planets in our solar system and beyond obey this law shown in this work, namely that gases and liquids are more or less restrained from flowing outwards of the surface of a given planet (such as earth for example) as space is a near perfect vacuum surrounding the planets it makes physical sense that this is true. Why? Because of universal gravitation which acts as an external force to the flow of gases and liquids within the planets and keeps an atmospheric circulation zone intact and attached to the surface of the sphere of a given planet. The 3-Torus is the easiest 3-manifold to understand. In 1984, Alexei Starobinsky and Yakov Zeldovich at the Landau Institute in Moscow proposed a cosmological model where the shape of the universe is a 3-torus. To visualize the three-torus, we can obtain it by gluing just like the two-Torus: We start with a cube, and glue each face of the cube to the parallel face, by parallel translation. (See Thurston [19] on how to visulaize a three-Torus) In this cosmological structure that is being proposed again it is true that there is a separation of two main regions of highly turbulent flow. So we partition the flow dynamics in two areas of such cubes of the 3-Torus, namely inside and outside the sphere. The Hölder continuous function for v_3 on the ball of radius 1 proves that acceleration can be arbitrarily large on the ball. Existence of non Hölder solutions on the ball is reserved for future work. For Dirichlet boundary conditions on the sphere existence and uniqueness of solutions may be possible [6]. The no-flux condition proves that there is an equilibrium condition that turbulence adjusts or sets to. Observing inside the spherical windows we see that there may exist infinitely many eddies and whirls. Now what can be said about the exterior of the sphere for all spheres in the lattice? Here one has to solve numerically for the flow problem of PNS in the corners of the cubes where there exist 8 vertices each with a cone surface for each cube in the lattice. It seems that there would be some flow interaction between all corners of the cubes and outside the spheres. So there can be trajectories confined within the sphere and outside of the sphere chaotic trajectories interacting with a

multitude of corners in the lattice.

6. Conclusion

In this paper, it has been determined that as the kinematic viscosity changes from the corresponding value at $\nu = 0$ to the fully viscous case for the Periodic Navier Stokes equations (PNS) at the value $\nu = 1$ the solution reaches a peak ($\frac{\partial v_3}{\partial y_3} = 0$) in y_3 (the third component of $\boldsymbol{r} = (y_1, y_2, y_3)$ in Cartesian coordinates). Here in the viscous case, there exists a dipole which is not centered at the center of the cell of the Lattice. This immediately implies that since the dipole by definition has an equal in magnitude positive and negative peak in the third component of velocity, then the dipole Riemann cut-off surface is covered by a closed surface which is the sphere $\|\boldsymbol{r}\| = 1$ and where a given cell of dimensions $[-1,1]^3$ is circumscribed on a sphere of radius 1. For such a closed surface containing a dipole, it necessarily follows that the flux at the surface of the sphere of v_3 wrt to surface normal $\boldsymbol{n}$ is zero. In terms of mathematical analysis of the NS equations in a thin spherical shell, the convergence of the longitudinal velocity averaged in the radial direction across the shell to the strong solution to the two-dimensional NS equations on a sphere as the thickness of the shell converges to zero has been rigorously proved by Temam and Ziane. However a Dirichlet type impenetrability condition is used there with all three components of velocity (no gradients at the wall). In the present work a Neumann impenetrability condition is used with the gradient of the third component of velocity. Here at the six points where the sphere touches the cube walls, it has been determined that the velocities satisfy PNS and the function v_3 is Hölder continuous there. By using the spherical coordinate system in terms of Cartesian coordinates and using the chain rule the solution can be extended to all of the spheres. This is the first extension. Finally as a result of the present work, on the sphere with a Neumann boundary condition, (Here $\frac{\partial v_3}{\partial \boldsymbol{n}} = \boldsymbol{n} \cdot \nabla v_3$) a non smooth solution [8] for v_3 exists which is Hölder continuous and it is proven that it is possible to extend Hölder continuity on the sphere uniquely to all of the interior of the Ball of radius one. Although non-uniqueness is proposed to occur for solutions in the interior of the ball for PNS equations, there exists at least one solution there that is Hölder continuous. In the present study, a point vortex at the center of the cells exists with a finite time singularity for Euler's equation for derivatives of the velocities and as the kinematic viscosity changes from zero to one (maximum) then there is a surface vortex first derivative singularity along an atmospheric circulation layer. The inner part of this layer touching the surface of a planet is the sphere. The fluid below this sphere of the atmosphere is a viscous fluid. This is evident by looking at **Figure 1** and **Figure 2** and **Figure 4**. There the dipole centre is not touching this sphere layer. The model proven in this paper has cosmological applications which are justified by PNS equations.

Acknowledgements

Sincere thanks to Cindy Zhang Managing Editor of APM, and special thanks to reviewers for helpful comments.

Conflicts of Interest

The author declares no conflicts of interest regarding the publication of this paper.

References

[1] Alexakis, A. and Biferale, L. (2018) Cascades and Transitions in Turbulent Flows. arxiv:1808.06186v2

[2] Kamruzzaman, M.D., Lyazid, D. and Antonia, R.A. (2023) Experimental Study of Two Side-by-Side Decaying Grid Turbulent Fields at Different Mean Velocities. *Journal of Turbulence*, **24**, Article 2182439. https://doi.org/10.1080/14685248.2023.2182439

[3] Khatar, M.M.A. (2023) Physics of Crystal Lattices and Plasma; Analytical and Numerical Simulations of the Gilson-Pickering Equation. *Results in Physics*, **44**, Article 106193. https://doi.org/10.1016/j.rinp.2022.106193

[4] Lydon, K., Nazarenko, S.V. and Laurie, J. (2022) Dipole, Dynamics in the Point Vortex Model. *Journal of Physics A: Mathematical and Theoretical*, **55**, Article 385702. https://doi.org/10.1088/1751-8121/ac89bc

[5] Provenzale, A. (1999) Transport by Coherent Barotropic Vortices. *Annual Review of Fluid Mechanics*, **31**, 55-93. https://doi.org/10.1146/annurev.fluid.31.1.55

[6] Wang, S. and Wang, Y. (2020) The Global Well-Posedness for Large Amplitude Smooth Solutions for 3D Incompressible Navier-Stokes and Euler Equations Based on a Class of Variant Spherical Coordinates. *Mathematics*, **8**, Article 1195. https://doi.org/10.3390/math8071195

[7] Temam, R. and Ziane, M. (1997) Navier-Stokes Equations in Thin Spherical Domains. *Contemporary Mathematics*, **209**, 281-314

[8] Fefferman, C.L. (2006) Existence and Smoothness of the of the Navier-Stokes Equation. https://www.claymath.org/wp-content/uploads/2022/06/navierstokes.pdf

[9] Moschandreou, T.E. and Afas, K.C. (2021) Existence of Incompressible Vortex-Class Phenomena and Variational Formulation of Rayleigh Plesset Cavitation Dynamics. *Applied Mechanics*, **2**, 613-629. https://doi.org/10.3390/applmech2030035

[10] Moschandreou, T.E. (2021) No Finite Time Blowup for 3D Incompressible Navier-Stokes Equations via Scaling Invariance. *Mathematics and Statistics*, **9**, 386-393. https://doi.org/10.13189/ms.2021.090321

[11] Moschandreou, T.E. and Afas, K.C. (2023) Periodic Navier-Stokes Equations for a 3D Incompressible Fluid with Liutex Vortex Identification Method. *Vortex Simulation and Identification*, 1-22. https://doi.org/10.5772/intechopen.110206

[12] Moschandreou, T.E. (2023) Exploring Finite-Time Singularities and Onsager's Conjecture with Endpoint Regularity in the Periodic Navier Stokes Equations. *Global Journal of Researches in Engineering*: *I Numerical Methods*, **23**, 45-59.

[13] Moschandreou, T.E. Afas, K. and Nguyen, K. (2024) Theoretical and Computational Fluid Mechanics: Existence, Blowup, and Discrete Exterior Calculus Algorithms. 1st Edition, Chapman and Hall/CRC, Boca Raton, USA, 1-338. https://doi.org/10.1201/9781003452256-1

[14] Leray, J. (1934) Sur le mouvement d'un liquide visqueux emplissant l'espace. *Acta Mathematica*, **63**, 193-248. https://doi.org/10.1007/BF02547354

[15] Yu, B.R. and Fet, A.I. (1970) Theory of Unitary Symmetry. Russian-Published, Moscow.

[16] Jeffrey, D. (2023) Branch Cuts and Riemann Surfaces. Arxiv:2302.13188, 1-7.

[17] Munkres, J.R. (2017) Topology, Pearson. 2nd Edition, Pearson, MIT, Massachusetts, USA.

[18] Suri, B., Tithof, J., Grigoriev, R.O. and Schatz, M.F. (2017) Forecasting Fluid Flows Using the Geometry of Turbulence. *Physical Review Letters*, **118**, Article 114501. https://doi.org/10.1103/PhysRevLett.118.114501

[19] Thurston, W.P. (1997) Three Dimensional Geometry and Topology, Volume 1. Princeton University Press, Princeton, 31. https://doi.org/10.1515/9781400865321